Structural basis for origin recognition complex 1 protein–silence information regulator 1 protein interaction in epigenetic silencing

Hao-Chi Hsu, Bruce Stillman, and Rui-Ming Xu*

Cold Spring Harbor Laboratory, Cold Spring Harbor, NY 11724

Contributed by Bruce Stillman, April 18, 2005

The interaction between silence information regulator 1 protein (Sir1p) and origin recognition complex 1 protein (Orc1p), the largest subunit of the origin recognition complex, plays an important role in the establishment of transcriptional silencing at the cryptic mating-type gene loci in *Saccharomyces cerevisiae*. Sir1p binds the N-terminal region of Orc1p encompassing a Bromo-adjacent homology (BAH) domain found in various chromatin-associated proteins. To understand the molecular mechanism of Sir protein recruitment, we have determined a 2.5-Å cocrystal structure of the N-terminal domain of Orc1p in complex with the Orc1p-interacting domain of Sir1p. The structure reveals that Sir1p Orc1p-interacting domain has a bilobal structure: an α/β N-terminal lobe and a C-terminal lobe resembling the Tudor domain royal family fold. The N-terminal lobe of Sir1p binds in a shallow groove between a helical subdomain and the BAH domain of Orc1p. The structure provides a mechanistic understanding of Orc1p–Sir1p interaction specificity, as well as insights into protein–protein interactions involving BAH domains in general.

structure | transcriptional silencing

Epigenetic control of gene expression involves the assembly of higher order chromatin structures. In the budding yeast *Saccharomyces cerevisiae*, cryptic mating-type genes, *HML* and *HMR*, are epigenetically silenced. Genetic and biochemical studies have identified cis- and trans-acting factors required for the establishment and maintenance of transcriptional silencing at the *HM* loci (1). The silent *HM* loci are flanked by specific cis-acting DNA sequences called the E and I silencers, which contain two or more binding sites for DNA-binding proteins, the origin recognition complex (Orc), Rap1p, and Abf1p (2–6). Silencing at the *HM* loci also requires four silent information regulator (Sir) proteins, Sir1p, Sir2p, Sir3p and Sir4p (7, 8).

Orc is a six-protein complex important for initiation of DNA replication and transcriptional silencing (2, 9, 10). The N-terminal domain (NTD) of Orc1p, the largest subunit of Orc, is specifically required for transcriptional silencing at the *HM* loci (11). The NTD of Orc1p is ≈220 residues in length, and it shares ≈50% amino acid identity with the N-terminal region of Sir3p. The NTD of Orc1p interacts with Sir1p, and this interaction is important for recruiting other SIR proteins to the *HM* loci as Sir1p also interacts with Sir4p (12). In *HM* and telomeric silencing, Sir4p forms a complex with Sir2p, and the Sir2p/Sir4p complex is joined by Sir3p (13–15). Sir2p is a NAD-dependent histone deacetylase (16–18), whereas Sir3p and Sir4p appear to have structural roles. Sir3p and Sir4p can self-associate, interact with Rap1p, and bind to the N-terminal tails of histone H3 and H4 (19, 20). This complex network of protein–protein interactions is responsible for the assembly of repressive higher-order chromatin structures at the *HM* loci.

The NTD of Orc1p contains a bromo-adjacent homology (BAH) domain (21), which is also present in a number of other chromatin-associated proteins, such as Sir3p, the predominant mammalian DNA methyltransferase DNMT1, the yeast RSC nucleosome remodeling complex subunits RSC1 and RSC2, and the MTA1 subunit of histone deacetylase complexes. We have previously determined the Orc1p NTD structure and discovered that the major Sir1p-interaction region is located in a helical subdomain (H-domain) tethered to the predominant β-sheet BAH domain (22). The Orc1p-interacting domain (OID) is located in the C-terminal region of Sir1p, and it contains no recognizable sequence motifs (12, 23, 24). Interestingly, Orc1 NTD in higher eukaryotes interacts with HP1, and this interaction is thought to be important for heterochromatin formation (25, 26). Thus, Orc1 NTD appears to have an evolutionarily conserved function of recruiting silencing proteins to chromatin, although the structural bases for these specific protein–protein interactions are poorly understood.

To understand the structural basis for Orc1p–Sir1p binding specificity and to provide insight into the mode of protein–protein interaction involving BAH domain proteins, we have determined a 2.5-Å structure of the Orc1p NTD in complex with Sir1p OID. The structure reveals that Sir1p OID has an α/β structure rich in β-strands. Sir1p OID binds in a cleft formed between the BAH domain and H-domain. The detailed structural information provides important insights into the mechanisms of heterochromatin formation in yeast.

Materials and Methods

Protein Methods. The Orc1p NTD–Sir1p OID complex was produced by coexpression in BL21(DE3) *Escherichia coli* cells using two T7 expression plasmids carrying the respective cDNA fragments. Sir1p OID (amino acids 480–612) was expressed as a C-terminal poly(histidine)-tagged protein by using a pET23a vector (Novagen). Orc1p NTD (amino acids 1–219) was expressed by using a pMR101 vector (American Type Culture Collection). Recombinant Orc1p NTD has a natural, untagged N terminus. The complex was purified by column chromatography on Hi-Trap Ni, Hi-Trap S, and Superdex-75 columns (AP-Biotech). The purified complex was concentrated to ≈46 mg/ml in a buffer containing 10 mM Tris (pH 6.8), 0.2 M NaCl, and 1 mM dithiotreitol for crystallization studies. Selenomethionine (SeMet)-substituted protein complex was expressed in a methionine-requiring auxotroph, DL41(DE3), by using a defined medium supplemented with SeMet (27). The SeMet Orc1p NTD–Sir1p OID complex was purified and crystallized in a manner similar to that used for the native protein complex.

Crystallographic Methods. The protein complex was crystallized by hanging-drop vapor diffusion in a condition containing 0.1 M Mes, pH 6.2, and 4.0 M NaCl. The crystal has an I222 symmetry

BIOCHEMISTRY

Abbreviations: Orc, origin recognition complex; Sir, silent information regulator; BAH, bromo-adjacent homology; OID, Orc1p-interacting domain; H-domain, helical subdomain; NTD, N-terminal domain; SMN, survival motor neuron.

Data deposition: Atomic coordinates and diffraction data have been deposited in the Protein Bata Bank, www.pdb.org (PDB ID code 1ZBX).

*To whom correspondence should be addressed at: Cold Spring Harbor Laboratory, 1 Bungtown Road, Cold Spring Harbor, NY 11724. E-mail: xur@cshl.edu.

Table 1. Summary of crystallographic analysis

Data sets	Native	K_2PtCl_4	Se inflection	Se peak
Resolution, Å	2.4	2.8	3.0	3.0
Measured reflections	221,761	244,037	164,458	184,393
Unique reflections	26,351	18,210	13,988	13,783
Average I/σ	21.1	24.0	15.8	13.8
Completeness, % ($I/\sigma > 0$)	94.3 (85.5)	97.0 (98.6)	96.4 (89.6)	97.3 (92.4)
R_{merge}, %*	5.4 (39.6)	8.2 (17.5)	6.8 (35.7)	8.0 (30.4)
Phasing power (iso/ano)†	—/—	1.62/1.49	—/0.81	1.07/2.03
Figure of merit	—	0.39		0.45
Refinement				
Resolution range, Å	50.0–2.5			
R_{factor}/R_{free}, %‡	22.0/26.0			
Protein atoms, *n*	2,612			
Water molecules, *n*	164			
rms deviations				
Bond lengths, Å	0.007			
Bond angles, °	1.41			

—; not applicable.

*$R_{merge} = \Sigma|I - \langle I\rangle|/\Sigma\langle I\rangle$, where I and $\langle I\rangle$ are the averaged intensity of multiple measurements of the same reflection. The summation is over all the observed reflections.

†Phasing power = rms ($\langle F_H\rangle/E$), where F_H is the calculated structure factor of the heavy atoms and E is the residual lack of closure. Isomorphous (iso) and anomalous (ano) contributions are separately shown.

‡$R_{factor} = \Sigma||F_o| - |F_c||/\Sigma|F_o|$, where F_o denotes the observed structure factor amplitude and F_c denotes the structure factor calculated from the model.

with cell dimensions of $a = 70.00$ Å, $b = 137.21$ Å, and $c = 139.77$ Å. All diffraction data were collected at 100 K at the X26C beamline of the National Synchrotron Light Source (Brookhaven National Laboratory, Upton, NY). Data were processed by using the HKL program (28), and the statistics are shown in Table 1. The crystals appear to be sensitive to radiation damage during a prolonged period of data collection.

The structure was solved by combining the phases obtained from three sources: (*i*) molecular replacement by using the Orc1p NTD structure (Protein Data Bank ID code 1M4Z) as a search model; (*ii*) two-wavelength anomalous diffraction from a selenomethionine crystal; and (*iii*) single-wavelength isomorphous and anomalous scattering data from a Pt derivative (obtained by soaking a native crystal in the presence of 2 mM K_2PtCl_4 for 6 h). The three sets of phases were combined and extended to 2.5-Å resolution with iterative cycles of solvent flattening and phase recombination by using the PHASES program suite (29). Model building was carried out by using the graphic program O (30), and structure refinement was carried out by using CNS (31). Phasing and refinement statistics are shown in Table 1. Figures were prepared with the programs MOLSCRIPT (32), RASTER3D (33), and PYMOL (34).

Results and Discussion

Phase combination and extension produced a high-quality electron density map (Fig. 1*A*), which allowed unambiguous assignment of Orc1p NTD (amino acids 1–219) and Sir1p OID (amino acids 480–612) residues (Fig. 1*B*). Sir1p and Orc1p each contain a disordered internal segment: residues 578–588 in Sir1p and residues 22–36 in Orc1p. The refined structure has good stere-

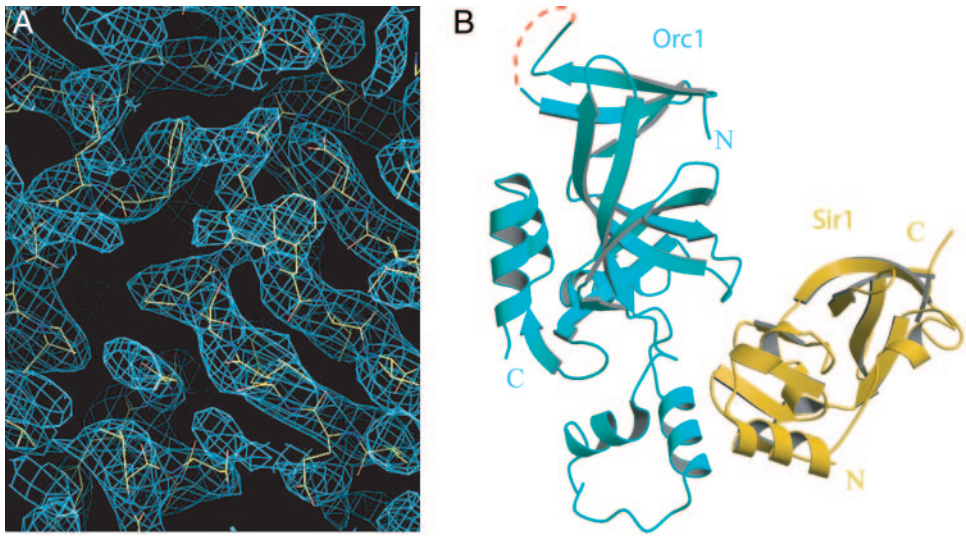

Fig. 1. Structure determination. (*A*) A section of phased-extended electron density map surrounding the Orc1p NTD–Sir1p OID interface. The 2.5-Å electron density map is contoured at 1.0 σ level. (*B*) A ribbon diagram showing the overall structure of the Orc1p NTD–Sir1p OID complex. Orc1p is shown in cyan, and Sir1p is shown in yellow. Red dashed lines indicate disordered loops.

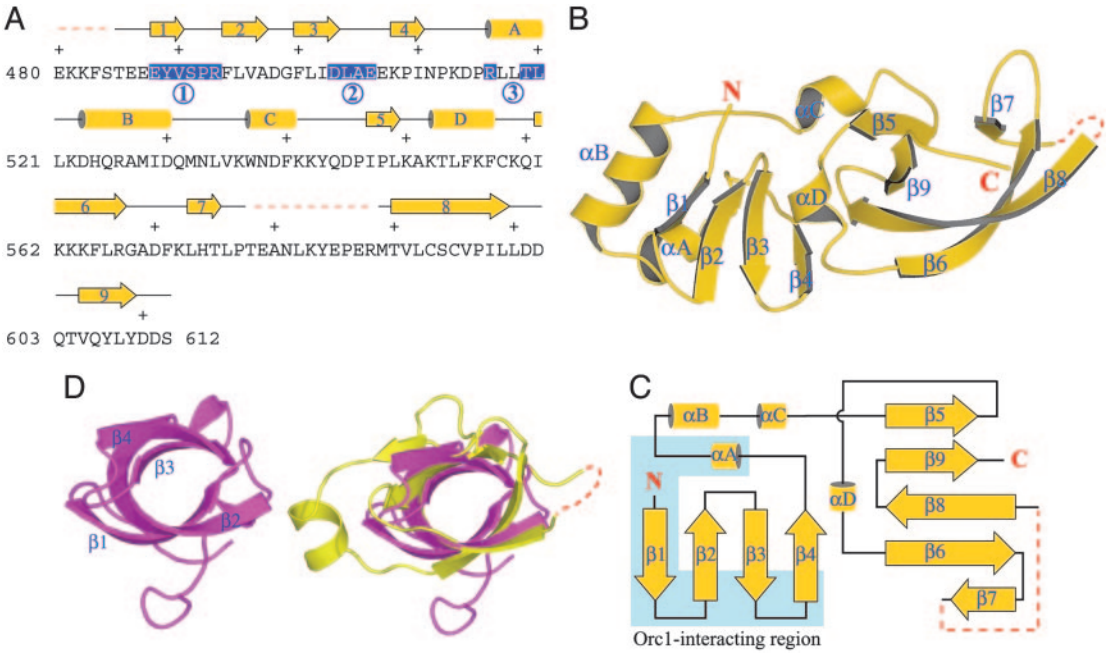

Fig. 2. Sir1p OID structure. (*A*) Sequence and secondary structure of Sir1p OID. Red dashed lines indicate disordered regions in the crystal structure. A plus sign is shown above the sequence to indicate every 10 residues. Three Orc1p-interacting regions, indicated by encircled numbers, are shown as white letters over a blue background. (*B*) Sir1p OID structure shown in a ribbon representation. Secondary structure elements are labeled. (*C*) A schematic drawing of the folding topology of Sir1p OID. The shaded region is involved in Orc1p binding, and the dashed red line indicates a disordered loop. (*D*) The C-terminal lobe of Sir1p OID has a Tudor-like structure. (*Left*) The SMN Tudor domain is shown in a ribbon representation. (*Right*) A superposition of the C-terminal lobe of Sir1p OID (yellow) with the SMN Tudor domain.

ochemical quality: 86% of the main chain ϕ/ψ angles are in the most favored region, and none in the disallowed region of the Ramachandran plot, calculated by using PROCHECK (35).

Structure of Sir1p OID. Sir1p OID does not have any recognizable sequence motifs that can aid the understanding of Orc1p–Sir1p interaction (Fig. 2*A*). The crystal structure reveals that Sir1p OID is folded into an elongated structure rich in β-strands (Fig. 2*B*). The structure consists of two topologically separable lobes packed against each other (Fig. 2*C*). The N-terminal lobe is formed by four antiparallel β-strands (β1–β4) and two helices (αA and αB). The two helices are packed against the same side of the β-sheet (Fig. 2*B*). The C-terminal lobe consists of five antiparallel β-strands (β5–β9) that are arranged in a tubular structure. Additionally, two short helices (αC and αD) flank the first strand, β5, in the C-terminal lobe (Fig. 2*B*). Helix αD appears to be important for stabilizing the packing of the two Sir1p OID lobes, because it interacts extensively with amino acids located at one side (opposite to the side occupied by αA and αB) of the N-terminal β-sheet (Fig. 2*B*).

The overall fold of Sir1p OID does not resemble any known structures, because structural similarity searches using the DALI server did not yield significant matches. It is clear from the cocrystal structure that the N-terminal lobe is involved in the interaction with Orc1p (Fig. 1*B*). The distinct tubular arrangement of the β-strands in the C-terminal lobe is reminiscent of a Tudor-like structure. Fig. 2*D* shows the Tudor domain structure of survival motor neuron (SMN), the spinal muscular atrophy protein (36). The Sir1p C-terminal lobe superimposes well with the SMN Tudor domain. The two structures have a rms deviation of 1.06 Å, using 20 residues on β6, β8, and β9 of Sir1p OID for alignment with corresponding residues on β1, β2, and β3 of the SMN Tudor domain, respectively. Tudor and related domains form a so-called "royal family" of domains that function in protein–protein interactions, sometimes by means of methylated arginine or lysine residues (37). It is interesting that Sir1p, like many other chromatin-associated proteins, contains a domain of the Tudor domain royal family, which suggests that the Sir1p Tudor-like domain may also have a function in protein–protein interactions.

Structure of Orc1p NTD. Orc1p NTD contains a core BAH domain that consists mainly of β-strands and a helical H-domain that is important for Sir1p-binding (22). Two antiparallel α-helices located at the C terminus of Orc1p NTD pack against the BAH domain and appear to be important for stabilizing the mainly β-sheet BAH fold (Fig. 3). Comparing the Sir1p-bound Orc1p structure with that of the free Orc1p NTD reveals two main differences: (*i*) Nine residues at the N terminus of Orc1p have a very different conformation, and (*ii*) helix αD and the preceding loop in the H-domain move toward the bound Sir1p in the present structure. The N-terminal end of αD shifted by $\approx$4 Å.

The difference in the N terminus appears to be due to self-interaction between Orc1p NTD molecules in the crystal lattice. In the structure of Orc1p NTD alone, the N-terminal tail of approximately 8 to 10 residues is involved in the interaction between two Orc1p NTD molecules within the same asymmetric unit (22). This region is also involved in protein–protein interactions between two symmetry-related Orc1p NTD molecules in the present structure, but the way they interact has changed. In the present structure, the N terminus of Orc1p starts at Ala-2; the initiating formyl-methionine is likely removed by cotranslational processing during expression. Orc1p NTD crystallized alone was with a construct having four artificial amino acids at the N terminus (22). This amino acid difference may contribute to the altered conformation of the N terminus of Orc1p in the two structures.

The movement of αD and adjacent loops in the H-domain appears to be induced by the binding of Sir1p OID (Figs. 1*B* and 4). Sir1p contacts three Orc1p regions: region I encompassing

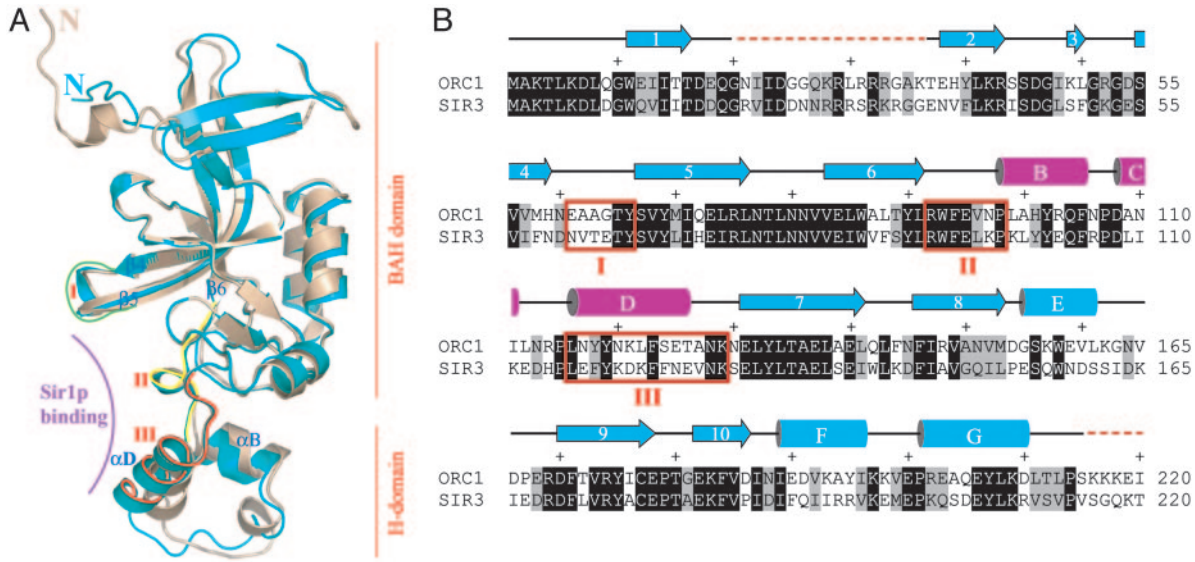

Fig. 3. Orc1p NTD structure. (*A*) Superposition of Orc1p NTD structures of that in the presence (cyan) or absence (beige) of Sir1p OID. In the orientation shown, the BAH domain is on top and the H-domain is at the bottom. The Sir1p NTD-binding cleft is indicated with a purple arc. Three regions involved in Sir1p binding are indicated with green (region I), yellow (region II), or red (region III) traces. (*B*) Alignment of Orc1p and Sir3p NTD sequences. Orc1p NTD secondary structures, with those in the H-domain shown in red, are indicated above the sequences. Dashed red lines indicate disordered regions. Three Sir1p-interacting Orc1p segments are enclosed in red boxes, and the three regions are labeled with roman numerals.

residues 61–66, which is located in the BAH domain; region II spanning residues 92–98, which is on the loop connecting β6 of the BAH domain with αB in the H-domain; and region III consisting of αD and the following loop (Fig. 3*B*). Amino acids in the three regions form a Sir1p-binding cleft (Figs. 3*A* and 4).

Orc1p–Sir1p Interaction. Sir1p interacts with Orc1p mainly through residues located in three regions of the Sir1p OID: (*i*) β1-turn-β2, (*ii*) β3-turn-β4, and (*iii*) three residues on αA (Fig. 2*A*). These residues are all located in the N-terminal lobe of Sir1p OID, and they contact Orc1p residues in the cleft formed between the BAH and H-domains (Fig. 4*A*). This interaction buries 1,046 Å^2 of protein surface area, which is within the range of surface areas common to specific and stable protein–protein interactions observed in many crystal structures. In the first Orc1p-interacting region (Fig. 2*A*), Pro-492^{Sir1}, Arg-493^{Sir1}, and Tyr-489^{Sir1} (Orc1p and Sir1p amino acids will be distinguished by a superscript hereafter) interact with Orc1p by means of hydrophobic and hydrogen bond interactions, whereas the rest of the amino acids in this region contact Orc1p through van der Waals interactions. Pro-492^{Sir1}and Arg-493^{Sir1} are located at the apex of the β1–β2 turn, and they make important contacts with Orc1p. Fig. 4*B* shows that Pro-492^{Sir1} binds in a shallow hydrophobic pocket formed by Trp-93^{Orc1}, Phe-94^{Orc1}, Val-96^{Orc1}, and Pro-98^{Orc1} located in the N-terminal loop connecting the BAH domain with the H-domain (region II), and Asn-120^{Orc1} and Phe-123^{Orc1} of helix αD in the H-domain (region III). The aliphatic portion of the Arg-493^{Sir1} side chain packs against Phe-94^{Orc1}, and the guanidinyl group of Arg-493^{Sir1} makes hydrogen bonds with the carbonyl groups of Ala-63^{Orc1} and

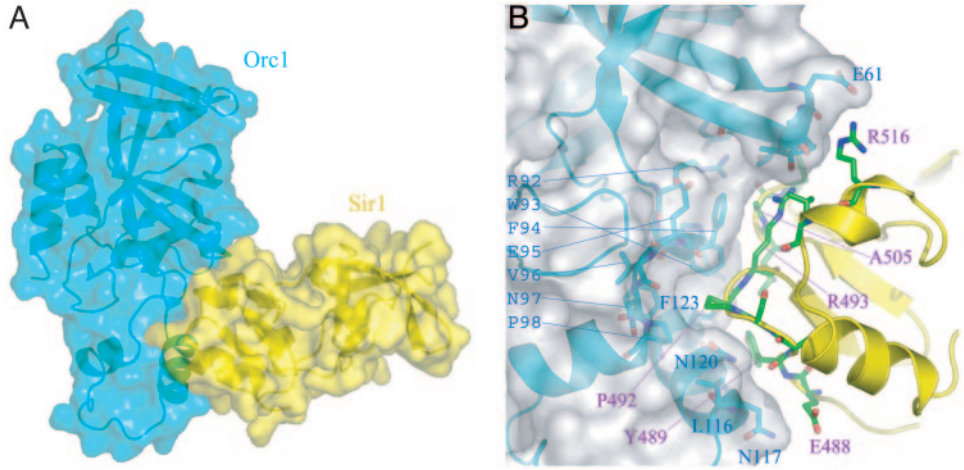

Fig. 4. Orc1p–Sir1p interaction. (*A*) A surface representation of the Orc1p NTD–Sir1p OID complex. Orc1p NTD and Sir1p OID are shown in semitransparent surfaces (cyan and yellow, respectively) superimposed with their respective ribbon models. (*B*) A detailed view of the protein interface. Orc1p NTD is shown in a surface representation superimposed with the ribbon model (cyan) and a stick model of residues interacting with Sir1p (cyan, carbon; blue, nitrogen; and red, oxygen). Sir1p OID is shown as a ribbon model (yellow) superimposed with a stick model of residues interacting with Orc1p (green, carbon; blue, nitrogen; and red, oxygen). Orc1p and Sir1p residues are indicated with cyan and magenta labels, respectively.

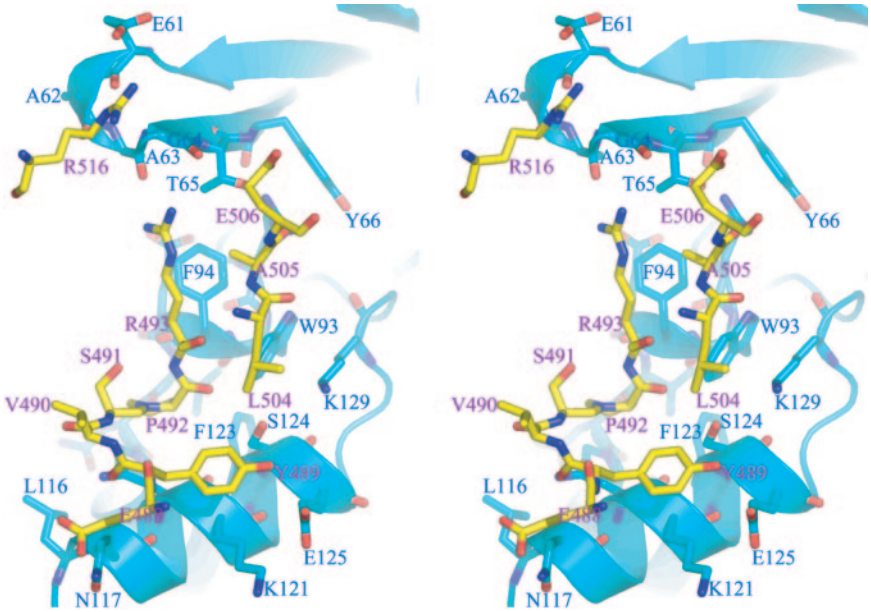

Fig. 5. A stereo view of Orc1p–Sir1p interaction. The protein interface is viewed from an angle approximately perpendicular to that in Fig. 4*B* (i.e., as from right to left in Fig. 4*B*). Orc1p is shown as a ribbon model superimposed with a stick model of relevant residues. Sir1p residues involved in interaction with Orc1p are shown in a stick model. A same coloring scheme as in Fig. 4*B* is used here.

Gly-64^{Orc1} (Figs. 4*B* and 5). Tyr-489^{Sir1} is located in β1, and its ring is packed against the aliphatic portion of Lys-121^{Orc1} (Fig. 5). Furthermore, the hydroxyl group of Tyr-489^{Sir1} interacts with Ser-124^{Orc1} and Lys-129^{Orc1} through a water molecule.

Leu-504^{Sir1}, Ala-505^{Sir1}, and Glu-506^{Sir1} in the second Orc1p-interaction region directly interact with Orc1p (Fig. 5). Leu-504^{Sir1} and Ala-505^{Sir1} interact with Orc1p hydrophobically through the packing of Leu-504^{Sir1} with Trp-93^{Orc1} and Ala-505^{Sir1} with Phe-94^{Orc1} and Thr-65^{Orc1}. Additionally, the carbonyl group of Ala-505^{Sir1} forms a hydrogen bond with Arg-92^{Orc1}. Glu-506^{Sir1} makes a hydrogen bond with the hydroxyl group of Thr-65^{Orc1}. The third Orc1p-interacting region is located in αA: Arg-516^{Sir1} makes two hydrogen bonds with the side chain oxygen atom and the main chain carbonyl of Glu-61^{Orc1}, whereas Thr-519^{Sir1} interacts with the carbonyl of Ala-62^{Orc1} through a water molecule, and Leu-520^{Sir1} and Ala-63^{Orc1} are in van der Waals contacts.

Specificity of Orc1p–Sir1p Interaction. Our previous structural, biochemical, and genetic studies indicated that the H-domain of Orc1p NTD is important for interaction with Sir1p (22). The Orc1p interaction region in Sir1p has also been mapped by genetic and biochemical methods (24). The cocrystal structure presented here directly confirms the results of these earlier studies and provides insights into the mode of Orc1p–Sir1p interaction. First, this study identifies a region in the BAH domain that encompasses Orc1p residues 61–66 (Fig. 3*B*, region I), to be important for the interaction between Orc1p and Sir1p. Second, the structure enables the precise identification of Sir1p-interaction regions within the H-domain (Fig. 3*B*, regions II and III), which is important for understanding the specificity of Orc1p–Sir1p interactions.

A great deal about the Orc1p–Sir1p interaction specificity is learned from comparing the structure with the knowledge gained from biochemical and genetic studies of Orc1p and Sir3p. An interesting observation is the that Orc1p NTD is highly homologous to Sir3p NTD, and the two domains are functionally interchangeable in *HM* silencing when tethered to the rest of Orc1p or Sir3p (11, 38). However, Sir3p NTD is not known to interact with Sir1p (38). Previously, we constructed a Sir3p–Orc1p swap (SOS) mutant replacing the putative Sir3p H-domain (amino acids 96–130) with that of the Orc1p H-domain (Fig. 3*B*). The SOS mutant of Sir3p gains the ability to interact with Sir1p (22), which suggests that Orc1p region I is unlikely to be a major determinant of Sir1p binding because this region is the same in the wild type and SOS mutant of Sir3p. The present cocrystal structure also rules out region II as a major determinant of Sir1p binding specificity because the only two residues different between Orc1p and Sir3p in this region are not involved in Sir1p binding. Examination of the structure suggests that residues Asn-117^{Orc1}, Asn-120^{Orc1}, Lys-121^{Orc1}, and Ser-124^{Orc1} in helix αD are likely to be major determinants of Sir1p binding specificity, because they directly interact with Sir1p in the structure and Sir3p has different amino acids at the corresponding positions, which may account for Sir3p's inability to interact with Sir1p OID. Asn-117^{Orc1} is unlikely to play a significant role because it interacts with Sir1p only weakly through van der Waals contacts, which is consistent with our previous observation that an alanine substitution of Asn-117^{Orc1}, together with alanine substitutions of several other H-domain residues, has no *HMR* silencing defects (online supplementary material of ref 22). Thus, this analysis concludes that Asn-120^{Orc1}, Lys-121^{Orc1}, and Ser-124^{Orc1} are important for Sir1p binding. A testable prediction would be that a Sir3p mutant replacing Lys-120^{Sir3}, Asp-121^{Sir3}, and Phe-124^{Sir3} with the corresponding Orc1p residues should gain the ability to interact with Sir1p OID.

Previous genetic analysis of Sir1p mutations that are defective in silencer recognition demonstrated the requirement of key amino acids (Tyr-489^{Sir1}, Val-490^{Sir1}, Ser-491^{Sir1}, Arg-493^{Sir1}, and Ala-505^{Sir1}) for interaction with Orc1p (23). These residues are located in the Orc1p-interacting regions identified from the structural study presented here (Fig. 2*A*). A more recent study identified seven additional amino acids (Phe-494^{Sir1}, Leu-501^{Sir1}, Asp-503^{Sir1}, Leu-504^{Sir1}, Trp-537^{Sir1}, Cys-595^{Sir1}, and Leu-608^{Sir1}) as being required for the interaction (24). All of these residues, except Asp-503^{Sir1}and Leu-504^{Sir1}, play a structural role of the Sir1p OID domain. Leu-504^{Sir1} interacts with Trp-93^{Orc1}

(Fig. 5) and Asp-503^{Sir1} interacts with Orc1p by means of van der Waals contact with Gly-64^{Orc1}. Another important role of Asp-503^{Sir1} is to stabilize the side chain conformation of Arg-493^{Sir1}, which is involved in multiple contacts with Orc1p.

Our structural study also reveals a previously unknown third Orc1p-interacting region in helix αA. Sir1p has an interesting Orc1p-interacting mode: Two small residues, Pro-492^{Sir1} and Ala-505^{Sir1}, are situated at the tips of β-turn-β motifs and they spearhead the interaction with Orc1p by binding in two shallow hydrophobic pockets. The small size of the two residues is crucial because it allows ideal surface complementarity between the two interacting proteins. The C-terminal lobe of Sir1p does not interact with Orc1p (Fig. 4). We noted that the C-terminal lobe has a structure similar to the Tudor domain superfamily members, many of which have been implicated in protein–protein interactions (37). It is possible that the structural similarity also indicates a protein–protein interaction function of the Sir1p OID C-terminal lobe. It has been shown that Sir4p interacts with Sir1p through a region encompassing OID (24); thus, it is an attractive hypothesis that the Tudor-like structure of the C-terminal lobe is involved in interaction with Sir4p. Sir1p has also been shown to be part of the yeast centromeric chromatin, and it interacts with the largest subunit of chromatin assembly factor I (39). It would be interesting to know whether the recruitment of Sir1p to centromeres is also mediated through the OID.

We thank Annie Heroux and Dieter Schneider for help during data collection at the X26C beamline of the National Synchrotron Light Source of Brookhaven National Laboratory and Lee Henry for comments on the manuscript. The work was supported in part by the W. M. Keck Foundation (R.-M.X.) and by National Institutes of Health Grants GM 63716 (to R.-M.X.) and CA13106 and GM45436 (to B.S.).

1. Rusche, L. N., Kirchmaier, A. L. & Rine, J. (2003) *Annu. Rev. Biochem.* **72,** 481–516.
2. Bell, S. P. & Stillman, B. (1992) *Nature* **357,** 128–134.
3. Shore, D. & Nasmyth, K. (1987) *Cell* **51,** 721–732.
4. Diffley, J. F. & Stillman, B. (1989) *Science* **246,** 1034–1038.
5. Rhode, P. R., Sweder, K. S., Oegema, K. F. & Campbell, J. L. (1989) *Genes Dev.* **3,** 1926–1939.
6. Halfter, H., Kavety, B., Vandekerckhove, J., Kiefer, F. & Gallwitz, D. (1989) *EMBO J.* **8,** 4265–4272.
7. Ivy, J. M., Klar, A. J. & Hicks, J. B. (1986) *Mol. Cell. Biol.* **6,** 688–702.
8. Rine, J. & Herskowitz, I. (1987) *Genetics* **116,** 9–22.
9. Bell, S. P., Kobayashi, R. & Stillman, B. (1993) *Science* **262,** 1844–1849.
10. Fox, C. A., Loo, S., Dillin, A. & Rine, J. (1995) *Genes Dev.* **9,** 911–924.
11. Bell, S. P., Mitchell, J., Leber, J., Kobayashi, R. & Stillman, B. (1995) *Cell* **83,** 563–568.
12. Triolo, T. & Sternglanz, R. (1996) *Nature* **381,** 251–253.
13. Hecht, A., Strahl-Bolsinger, S. & Grunstein, M. (1996) *Nature* **383,** 92–96.
14. Moazed, D. & Johnson, D. (1996) *Cell* **86,** 667–677.
15. Moazed, D., Kistler, A., Axelrod, A., Rine, J. & Johnson, A. D. (1997) *Proc. Natl. Acad. Sci. USA* **94,** 2186–2191.
16. Imai, S., Armstrong, C. M., Kaeberlein, M. & Guarente, L. (2000) *Nature* **403,** 795–800.
17. Landry, J., Sutton, A., Tafrov, S. T., Heller, R. C., Stebbins, J., Pillus, L. & Sternglanz, R. (2000) *Proc. Natl. Acad. Sci. USA* **97,** 5807–5811.
18. Smith, J. S., Brachmann, C. B., Celic, I., Kenna, M. A., Muhammad, S., Starai, V. J., Avalos, J. L., Escalante-Semerena, J. C., Grubmeyer, C., Wolberger, C. & Boeke, J. D. (2000) *Proc. Natl. Acad. Sci. USA* **97,** 6658–6663.
19. Moretti, P., Freeman, K., Coodly, L. & Shore, D. (1994) *Genes Dev.* **8,** 2257–2269.
20. Hecht, A., Laroche, T., Strahl-Bolsinger, S., Gasser, S. M. & Grunstein, M. (1995) *Cell* **80,** 583–592.
21. Callebaut, I., Courvalin, J. C. & Mornon, J. P. (1999) *FEBS Lett.* **446,** 189–193.
22. Zhang, Z., Hayashi, M. K., Merkel, O., Stillman, B. & Xu, R. M. (2002) *EMBO J.* **21,** 4600–4611.
23. Gardner, K. A., Rine, J. & Fox, C. A. (1999) *Genetics* **151,** 31–44.
24. Bose, M. E., McConnell, K. H., Gardner-Aukema, K. A., Muller, U., Weinreich, M., Keck, J. L. & Fox, C. A. (2004) *Mol. Cell. Biol.* **24,** 774–786.
25. Pak, D. T., Pflumm, M., Chesnokov, I., Huang, D. W., Kellum, R., Marr, J., Romanowski, P. & Botchan, M. R. (1997) *Cell* **91,** 311–323.
26. Lidonnici, M. R., Rossi, R., Paixao, S., Mendoza-Maldonado, R., Paolinelli, R., Arcangeli, C., Giacca, M., Biamonti, G. & Montecucco, A. (2004) *J. Cell Sci.* **117,** 5221–5231.
27. Hendrickson, W. A., Horton, J. R. & LeMaster, D. M. (1990) *EMBO J.* **9,** 1665–1672.
28. Otwinowski, Z. & Minor, W. (1997) *Methods Enzymol.* **276,** 307–326.
29. Furey, W. & Swaminathan, S. (1997) *Methods Enzymol.* **277,** 590–620.
30. Jones, T. A., Zou, J. Y., Cowan, S. W. & Kjeldgaard, M. (1991) *Acta Crystallogr. A* **47,** 110–119.
31. Brunger, A. T., Adams, P. D., Clore, G. M., DeLano, W. L., Gros, P., Grosse-Kunstleve, R. W., Jiang, J. S., Kuszewski, J., Nilges, M., Pannu, N. S., *et al.* (1998) *Acta Crystallogr. D* **54,** 905–921.
32. Kraulis, P. J. (1991) *J. Appl. Crystallogr.* **24,** 946–950.
33. Merritt, E. A. & Bacon, D. J. (1997) *Methods Enzymol.* **277,** 505–524.
34. DeLano, W. L. (2002) PYMOL: A Molecular Graphics System (DeLano Scientific, San Carlos, CA).
35. Laskowski, R. A., MacArthur, M. W., Moss, D. S. & Thornton, J. M. (1993) *J. Appl. Crystallogr.* **24,** 946–956.
36. Sprangers, R., Groves, M. R., Sinning, I. & Sattler, M. (2003) *J. Mol. Biol.* **327,** 507–520.
37. Maurer-Stroh, S., Dickens, N. J., Hughes-Davies, L., Kouzarides, T., Eisenhaber, F. & Ponting, C. P. (2003) *Trends Biochem. Sci.* **28,** 69–74.
38. Stone, E. M., Reifsnyder, C., McVey, M., Gazo, B. & Pillus, L. (2000) *Genetics* **155,** 509–522.
39. Sharp, J. A., Krawitz, D. C., Gardner, K. A., Fox, C. A. & Kaufman, P. D. (2003) *Genes Dev.* **17,** 2356–2361.